ORIGINAL PAPER

Investigation of polyaniline films doped with Co^{2+} as the electrode material for electrochemical supercapacitors

Hui Xu · Jun-xia Wu · Chun-lei Li · Jun-long Zhang · Xiu-xiu Wang

Abstract H^+ and Co^{2+} ions co-doped polyaniline were synthesized by cyclic voltammetry onto the stainless steel mesh with various concentrations of cobalt chloride ($CoCl_2 \cdot 6H_2O$) in electrolyte. The structure and morphology of polyaniline (PANI) and $PANI/Co^{2+}$ films were characterized by Fourier transform infrared (FT-IR), X-ray diffraction (XRD), scanning electron microscopy (SEM), and X-ray photoelectron spectroscopy (XPS) techniques. The electrochemical properties of PANI and $PANI/Co^{2+}$ films were investigated by cyclic voltammetry, galvanostatic charge–discharge test, and electrochemical impedance spectroscopy (EIS) in 0.5 mol L^{-1} H_2SO_4 electrolyte in a three-electrode system. The PANI/0.3 M Co^{2+} film shows a larger specific capacitance of 736 F g^{-1} at a current density of 3 mA/cm^2 and lower resistance compared with the pure PANI film. The results indicated that the $PANI/Co^{2+}$ films are promising material for supercapacitors.

Keywords Nanomaterial · Cobalt ions · Supercapacitor · Specific capacitance

Introduction

Supercapacitors featuring high power density, high specific energy, and excellent long-term cyclability have currently drawn great interest in energy storage devices for their combinative advantages of rechargeable batteries and conventional capacitors [1–3]. Active materials are the most crucial factor in governing the electrochemical performance for supercapacitors. Generally, the active materials have three kinds including carbon materials [4, 5], conducting polymers [6, 7], and transition metal oxides [8, 9]. Among all these materials mentioned above, conducting polymers are the most promising materials as they possess redox pseudocapacitance in addition to double-layer capacitance. Conducting polymers offer the advantages of low cost compared with noble metal oxides and high charge capacity compared with carbon materials [10–12]. Among the available conducting polymers, polyaniline (PANI) has attracted much attention and been intensively studied as an electrode material owing to its unique proton doping/dedoping mechanism, intrinsic electrical conductivity, facile synthesis, and environmental stability [13–16].

PANI films are generally synthesized by different electrochemical methods in acid solutions containing aniline [17–19]. The doping/dedoping process involves redox reactions which are the basic of energy storage in doped PANI. The effect of protonic acid dopants on the properties of PANI has been widely investigated. In most cases, the ions of H^+ are originating from inorganic acids (HCl, H_2SO_4, $HClO_4$, etc.) [20, 21] and organic acids (such as p-toluene sulfonic acid) [22]. Recently, more and more attention has been focused on cations such as transition metal ions due to the unique electron exchange property of the combination. Li et al. [23] reported that H^+ and Zn^{2+} co-doped PANI show higher specific capacitance and better thermal stability. Dhibar et al. [24] synthesized PANI in pure and doped forms with various doping levels of $CuCl_2$ using in situ polymerization method, PANI in doped form shows a higher specific capacitance value of 626 F g^{-1} at a scan rate 10 mV s^{-1} with 2 wt% doping level and has higher thermal stability. In our previous works [25–27], we have investigated that PANI with different doping levels of Ni^{2+}, Zn^{2+}, and Cu^{2+} prepared by electrochemical polymerization in acid solution were with better electrochemical performance compared with pure PANI doped with H^+. H^+ and Ni^{2+} co-doped PANI films well demonstrated which

H. Xu (✉) · J.-x. Wu · C.-l. Li · J.-l. Zhang · X.-x. Wang
College of Petrochemical Technology, Lanzhou University of Technology, Lanzhou 730050, China
e-mail: xuhui@lut.cn

has a larger specific capacitance of 658.3 F g^{-1} at 5 mA cm^{-2} [26]. Meanwhile, H$^+$ and Zn^{2+} co-doped PANI films have the superhigh specific capacitance of 738 F g^{-1} at 5 mA cm^{-2} in H$_2$SO$_4$ electrolyte [27]. Thus, good capacitive performance demonstrates that PANI doped with transition metal ions may have potential superiority for the development of supercapacitors.

To study the effects of more transition metal ions on the electrochemical performance of PANI in detail, in this research, the PANI/Co^{2+} films were synthesized in HCl solution containing CoCl$_2$·6H$_2$O by cyclic voltammetry (CV) on low-cost stainless steel wire mesh substrates. The electrochemical properties of the PANI/Co^{2+} films were investigated by cyclic voltammetry, galvanostatic charge–discharge test, and electrochemical impedance spectroscopy (EIS) in a three-electrode system. The structure and morphology of PANI/Co^{2+} films were characterized by Fourier transform infrared (FT-IR), X-ray diffraction (XRD), scanning electron microscopy (SEM), and X-ray photoelectron spectroscopy (XPS) techniques, respectively.

Experimental

Materials Aniline was purified and stored at -5 $^{\circ}$C before use. All of the reagents purchased from Tianjin Chemical Industrial Co. Ltd. (Tianjin, China) were analytical grade and used without further purification. Double-distilled water was used for the preparation of solutions.

Electrochemical deposition of PANI and PANI/Co^{2+} The materials of PANI and PANI/Co^{2+} were prepared by cyclic voltammetric method in a classic one-compartment cell using three-electrode configuration on CHI660B electrochemical work station. Saturated calomel electrode (SCE) was used as reference electrode, platinum sheet was used as a counter electrode, and stainless steel wire mesh (type 316) was used as a working electrode for PANI deposition, which the deposited area was 1 cm^2 (1 cm$\times$1 cm) with other area insulated by a PTFE coating. In order to reduce stains on the surface, the stainless steel wire mesh was rinsed with acetone in ultrasonic bath for 10 min, immersed in ethanol ultrasonically for 10 min, and finally washed by distilled water, last air-dried for use. The cyclic voltammetry (CV) curves were recorded in a mixture of 0.5 mol L^{-1} (M) HCl and 0.2 mol L^{-1} aniline with different concentrations of 0.05, 0.1, 0.3, 0.5, and 0.8 mol L^{-1} CoCl$_2$·6H$_2$O at room temperature for 71 cycles by scanning the potential from -0.2 to 0.9 V at a scanning rate of 20 mV s^{-1}. After deposition, PANI/Co^{2+} films were rinsed with 0.5 mol L^{-1} HCl in order to remove soluble monomeric species and then dried under vacuum at 60 $^{\circ}$C for 12 h. The pure PANI film was prepared following the above process without CoCl$_2$·6H$_2$O and then obtained.

Characterization of the samples The samples used for structure characterizations were the powers scraped from PANI and PANI/Co^{2+} films on stainless steel wire mesh substrates. The structure was characterized by FT-IR (Nicolet, type210, America) which was recorded between 4000 and 500 cm^{-1}. The XRD patterns were characterized by D/MAX-2400X X-ray diffractometer with CuKα radiation ($\lambda=0.154056$ nm), employing a scanning rate of 10° min^{-1} in the 2θ range of 10–90°. The morphology of PANI and PANI/Co^{2+} were characterized by SEM (JEOL JSM-6701F). The XPS data were obtained by a V.G. ESCA Laboratory 210 photoelectron spectrometer with a MgKα source, the spectra were acquired with a 30-eV pass energy.

Electrochemical measurement Electrochemical studies were carried out in a three-electrode system. PANI and PANI/Co^{2+} films, a platinum electrode, and a saturated calomel electrode (SCE) were used as working electrode, counter electrode, and reference electrode, respectively. The electrochemical properties were evaluated by the cyclic voltammetry (CV), galvanostatic charge–discharge test (CP), and electrochemical impedance spectroscopy (EIS) in a glass cell with 0.5 mol L^{-1} H$_2$SO$_4$ aqueous solution as the electrolyte. Cyclic voltammetry and charge–discharge test were performed in the potential window ranging from 0 to 0.7 V vs. SCE. EIS measurements were recorded in the frequency range from 10^5 to 10^{-2} Hz with an excitation signal of 4 mV. All of the above electrochemical measurements were evaluated on a CHI660B electrochemical workstation (Chenhua, Shanghai, China).

Results and discussion

FT-IR Fig. 1 shows the FT-IR spectra of the pure PANI film and PANI/Co^{2+} film prepared in the solution with 0.3 mol L^{-1} Co^{2+}. The main characteristic peaks of PANI/Co^{2+} film were assigned as follows: the bands at 1558 and 1471 cm^{-1} were assigned to the N=Q=N stretching (Q represents the quinoid unit) and the N–B–N stretching (B represents the benzenoid unit), respectively. The bands located at 1297 and 1234 cm^{-1} were ascribed to C–N stretching vibration of quinoid rings and benzenoid rings, respectively. While the bands at 1116 and 802 cm^{-1} reflected the C–H in-plane deformation and out-of-plane vibration, respectively, from Fig. 1, we can see that some vibration frequencies of the PANI/Co^{2+} film are shifted to lower wavenumbers compared with those of the PANI film. The red shift of the IR absorption peaks is referred to be a signature of the conversion of the quinoid rings to the benzenoid rings by a proton-induced spin unpairing mechanism [28], which was considered to be an indication of increasing degree of charge delocalization on the PANI backbone [29]. It implies that PANI doped with Co^{2+} leads to an increase of
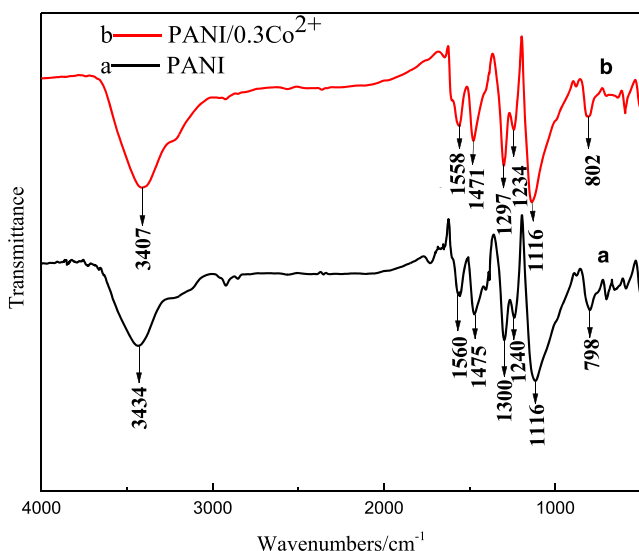
Fig. 1 FT-IR spectra of PANI (**a**) and PANI/Co^{2+} (**b**) films prepared in the solution with 0.3 mol L^{-1} Co^{2+}

charge delocalization on the PANI backbone compared to doping solely with HCl.

XRD Fig. 2 shows the XRD patterns of the PANI and PANI/0.3 M Co^{2+} films. One broad peak can be observed at $2\theta=25.42°$ from both of Fig. 2a, b, which were attributed to the characteristic peak of amorphous PANI. However, two other peaks at $2\theta=14.29°$ and $21.01°$ were observed from XRD pattern of PANI/0.3 M Co^{2+} film (Fig. 2b), which resulted in the periodicity parallel and perpendicular to the polymer chain [30]. This confirms lower crystallinity and conductive emeraldine salt structure of PANI.
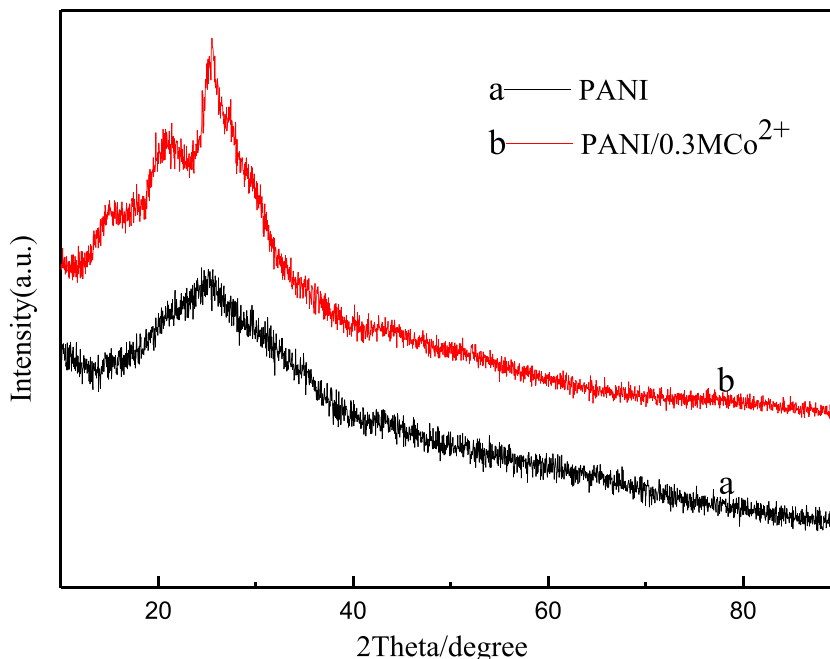
SEM The morphologies of PANI and PANI/0.3 M Co^{2+} films deposited on stainless steel mesh were measured by SEM, as shown in Fig. 3. As shown in Fig. 3a, the morphology of pure PANI exhibits a coral-like structure; meanwhile, PANI/0.3 M Co^{2+} film shows a quite similar structure (Fig. 3c). Also, from Fig. 3b, d, PANI/0.3 M Co^{2+} film shows a large, rough surface and nanostructure with nanorods, quite different from PANI; the pure PANI shows a surface with obviously few particles on its outside surface. The structure of PANI/0.3 M Co^{2+} may provide a larger surface area to volume ratio resulting in a high charge/discharge rate and specific capacitance. It is consistent with the results we drew from previous works [25–27], these indicate that the increased growth rate of PANI mainly depended on the presence of transition metal ions such as Ni^{2+}, Zn^{2+}, Cu^{2+}, and Co^{2+}, which could lead to further nucleation. It is probably because these transition metal ions have multiple doping positions proved by FT-IR which may bind to several nitrogen sites in a PANI chain or form inter-chain linkages among several adjacent PANI chains by coordination [31]. This organic–inorganic interaction is beneficial for supercapacitors, which leads to the decrease of the diffusion resistance of electrolyte into the electrode matrix.

X-ray photoelectron spectra The chemical bonding states of each element on the surface of PANI/0.3 M Co^{2+} are evaluated by XPS technique. Figure 4a shows the typical survey spectra of the PANI/0.3 M Co^{2+} film. From Fig. 4a, it announces that the deposit is composed of C, N, O, Cl, and Co elements without other obvious impurities. The obtained atomic weight percent of C1s, N1s, O1s, Cl2p, and Co2p in the PANI/0.3 M Co^{2+} film is 61.18, 10.04, 22.07, 6.1, and 0.6 %, respectively. Figure 4b shows the core level spectra of the Co2p region of

Fig. 2 XRD spectra of PANI (**a**) and PANI/Co^{2+} (**b**) films prepared in the solution with 0.3 mol/L Co^{2+}

Fig. 3 SEM images of PANI (*a, b*) film and PANI/ Co²⁺ (*c, d*) film prepared in the solution with 0.3 mol/L Co²⁺
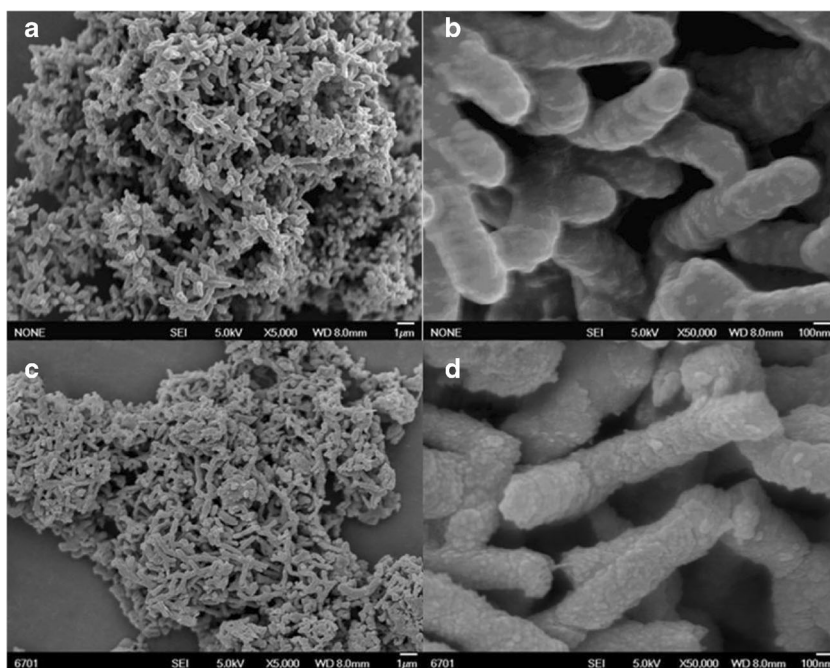
the sample. The Co 2p3/2, 2p1/2, and satellite peaks are computer fitted considering two spin–orbit doublets characteristic of Co^{2+} and Co^{3+}. The 2p3/2-to-2p1/2 separation of 15.7 eV and the very flat, weak satellite peaks indicate that the majority of cobalt is diamagnetic Co^{3+} [32].

Cyclic voltammetric test To evaluate the effect of Co^{2+} on the electrochemical characteristics of PANI film electrode for supercapacitors, current–potential response was employed in the potential range of 0 to 0.7 V versus SCE. Figure 5 illustrates the CV curves of PANI and PANI/Co^{2+} film electrodes at a scan rate of 3 mV s⁻¹ in 0.5 mol L⁻¹ H_2SO_4 electrolyte. The CV curves of PANI/Co^{2+} films were similar to those of PANI film and revealed a little deviation from a rectangular form, whereas some considerable differences were observed. The peak currents of the PANI/Co^{2+} film electrodes were relatively higher than those of PANI film, implying that a larger specific capacitance for the PANI/Co^{2+} film electrodes can be anticipated. This increase can be attributed to the redox process involved with Co^{2+}.

In order to further research the oxidation and reduction potentials and the properties of the PANI/Co^{2+} film electrodes, Fig. 6 shows the CV curves of the PANI/Co^{2+} film prepared in the solution with 0.3 mol L⁻¹ Co^{2+} at scan rates of 3, 5, 10, and 20 mV s⁻¹. In Fig. 6, three pairs of redox peaks (P_1/P_1', P_2/P_2', and P_3/P_3') can be observed. They were attributed to the redox process of PANI. Peak P_1/P_1' (0.27/0.01 V) corresponds to the oxidization of leucoemeraldine (LE) to emeraldine base (EM). Peak P_2/P_2' (0.54/0.37 V) is attributed to formation of PANI charge carriers consisting of polaron (radical cation) and bipolaron (dication) forms delocalized on PANI chains [33].

Peak P_3/P_3' (0.7/0.56 V) is due to the transformation of emeraldine to pernigraniline base (PE) [34]. With the increase of a scan rate from 3 to 20 mV s⁻¹, the redox peak current rapidly increased, indicating a good rate ability of the PANI/Co^{2+} film electrodes in 0.5 mol L⁻¹ H_2SO_4 electrolyte.

Galvanostatic charge–discharge experiments The galvanostatic charge–discharge studies are the most direct approach to evaluate the applicability of supercapacitors. The specific capacitance has been believed to approach to that of full utilization of the electrode material at low current density [35, 36], so we first measured the charge–discharge cycling at a constant current of 3 mA cm⁻². Figure 8 shows the typical charge–discharge curves of the PANI and PANI/Co^{2+}, which can be seen that the charge and the discharge profiles of the electrodes are slightly curved, exhibiting a pseudocapacitive characteristic, which is in good agreement with the results of CV curves. The specific capacitance (SC) values determined from the CP curves are calculated according to the following equation [25–27]:

$$Cm = I\Delta t/(m\Delta V)$$

where C_m is specific capacitance (F g⁻¹), I is charge/discharge current (A), Δt is the discharge time (s), ΔV is the potential drop in the discharge progress (V), and m denotes the mass of active material (5 mg). The calculated specific capacitances of PANI, PANI/0.05 M Co^{2+}, PANI/0.1 M Co^{2+}, PANI/0.3 M Co^{2+}, PANI/0.5 M Co^{2+}, and PANI/0.8 M Co^{2+} are attributed to 382, 419, 450, 736, 604, and 531 F g⁻¹, respectively. As shown in Fig. 7b, the specific capacitance of PANI and
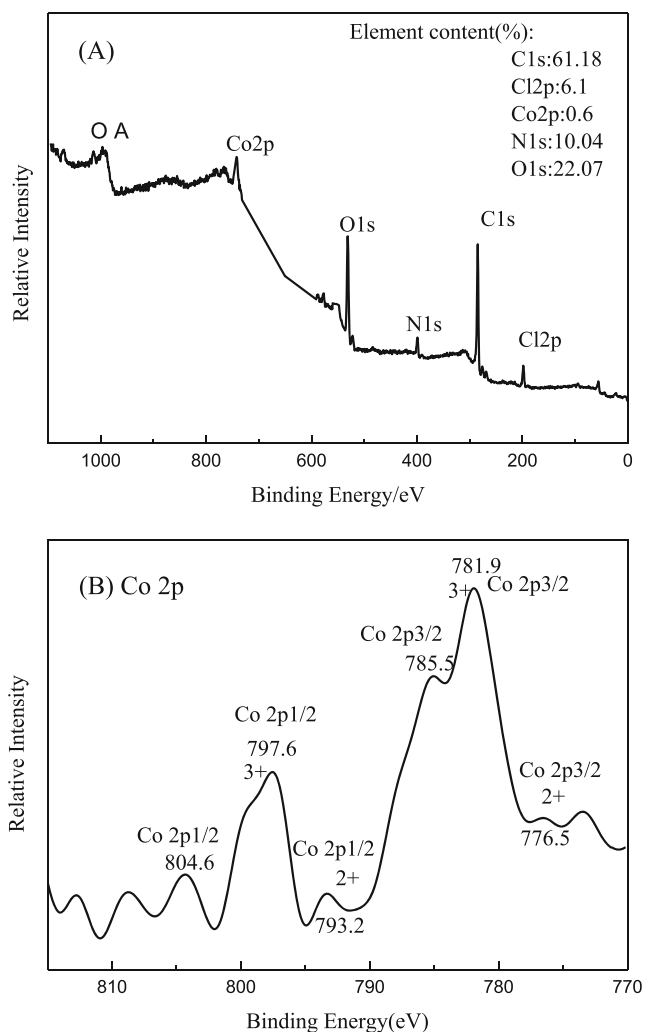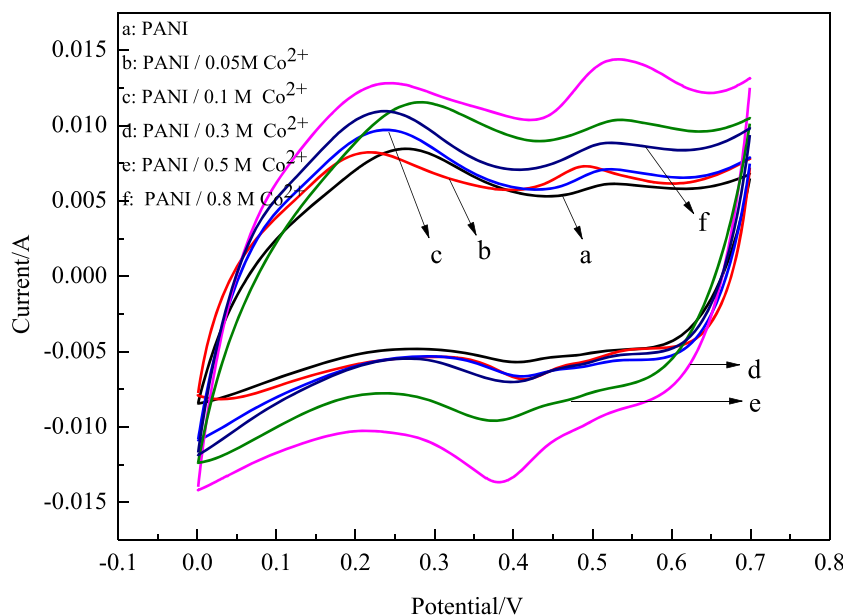
(A)

Element content(%):
C1s:61.18
Cl2p:6.1
Co2p:0.6
N1s:10.04
O1s:22.07

O A
Co2p
O1s
N1s
C1s
Cl2p

Relative Intensity

Binding Energy/eV

(B) Co 2p

781.9
3+ Co 2p3/2

Co 2p3/2
785.5

Co 2p1/2
797.6
3+

Co 2p3/2
2+
776.5

Co 2p1/2
804.6

Co 2p1/2
2+

793.2

Relative Intensity

Binding Energy(eV)

Fig. 4 **a** XPS survey spectra of the PANI/0.3 M Co^{2+} film. **b** Core level spectra of the Co 2p region

PANI/Co^{2+} films appeared increasing from 382 to 736 F g^{-1} with the increasing of Co^{2+} concentration in a range from 0 to 0.3 mol L^{-1} because Co^{2+} provides a least resistance path for electrons transferring. The improved performance is mainly attributed to the π–π interaction between Co^{2+} and PANI. Combined with our previous works [25–27], owing to the presence of transition metal ions, the PANI/M^{2+} (M=Ni, Cu, Zn, Co) films have an obvious improvement effect, which makes the PANI/M^{n+} films have more active sites for faradaic reaction than the pure PANI film and facilitates the charge–transfer of the PANI/M^{n+} films. However, with the further increasing of Co^{2+} concentration, the specific capacitance of PANI/Co^{2+} film occurred to be decreased, which is contributed to the covering of Co^{2+} onto the active sites of PANI.

The charge–discharge measurement of the PANI/0.3 M Co^{2+} (Fig. 7a) is also performed at various current density in 0.5 mol L^{-1} H_2SO_4 electrolyte, respectively. The related specific capacitances are calculated to be 736, 715, 662, and 571 F g^{-1} corresponding to the PANI/0.3 M Co^{2+} at current densities of 3, 5, 10, and 20 mA cm^{-2}, respectively. The anodic charge curves are almost mirror symmetrical to their cathodic discharge counterparts at each current density, indicating the PANI/0.3 M Co^{2+} electrode has a good electrochemical performance. With the increase of charge–discharge current densities, a potential drop has sharply increased due to the electrode polarization and the internal resistance [37]. In contrast, the IR drop is not obvious at relatively low current density.

In order to evaluate the stability of the electrodes, the charge–discharge cycling tests are conducted for 250 cycles, as shown in Fig. 7d. The variations of specific capacitances of PANI and PANI/0.3 M Co^{2+} films are performed at the current density of 3 mA cm^{-2}. Clearly, the specific capacitance retentions are retained at 43.4 and 58.1 % by contrary with the

Fig. 5 CV curves of PANI and PANI/Co^{2+} films at a scan rate of 3 mV s^{-1} in 0.5 mol L^{-1} H_2SO_4

a: PANI
b: PANI / 0.05M Co^{2+}
c: PANI / 0.1 M Co^{2+}
d: PANI / 0.3 M Co^{2+}
e: PANI / 0.5 M Co^{2+}
f: PANI / 0.8 M Co^{2+}

Current/A

Potential/V

Fig. 6 CV curves of PANI/Co^{2+} film prepared in the solution with 0.3 mol L^{-1} Co^{2+} in 0.5 mol L^{-1} H_2SO_4 at different scan rates
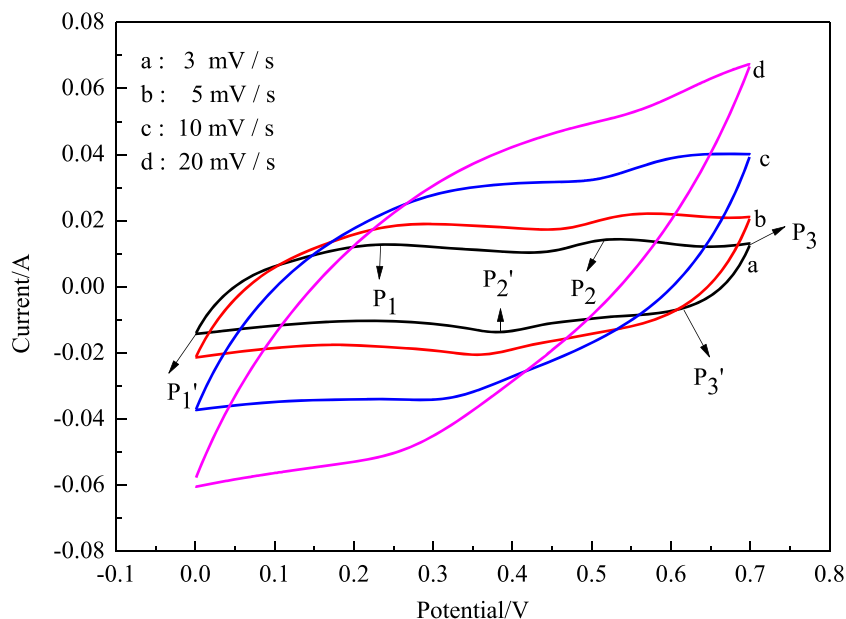
initial specific capacitances of PANI and PANI/0.3 M Co^{2+} films. The specific capacitances of whole prepared electrodes have an obvious decrease in the beginning, which is contributed to the degradation of incompletely formed polymer or some un-doped PANI. Compared with the specific capacitance retention of PANI, the Co^{2+} in the PANI/0.3 M Co^{2+} film has an important and positive effect to the cycleability of the PANI, due to the network or matrix of PANI chains with doping of Co^{2+} provides good synergy of volume changes

during the redox process, and the nanometer dimension of the electrode materials reduces the diffusion resistance of the electrolyte ions in the electrode. Compared with our previous works, we found that transition metal ions such as Ni^{2+}, Zn^{2+}, Cu^{2+}, and Co^{2+} did not have a direct effect of improving the stability of PANI. The transition metal ions doped PANI showed a relatively good stability and the improvement may be attributed to the redox process involved with transition metal ions, rough surface of nanorods structure, and

Fig. 7 a Charge–discharge curves of PANI and PANI/Co^{2+} films at a current density of 3 mA cm^{-2}. **b** Variation of specific capacitance with respect to Co^{2+} concentration at a current density of 3 mA cm^{-2}. **c** Charge–discharge curves of PANI/0.3 M Co^{2+} at various current densities. **d** Variations of discharge specific capacitance of PANI and PANI/0.3 M Co^{2+} films prepared in the solution with 0.3 mol L^{-1} Co^{2+} as a function of cycle number at 3 mA cm^{-2}
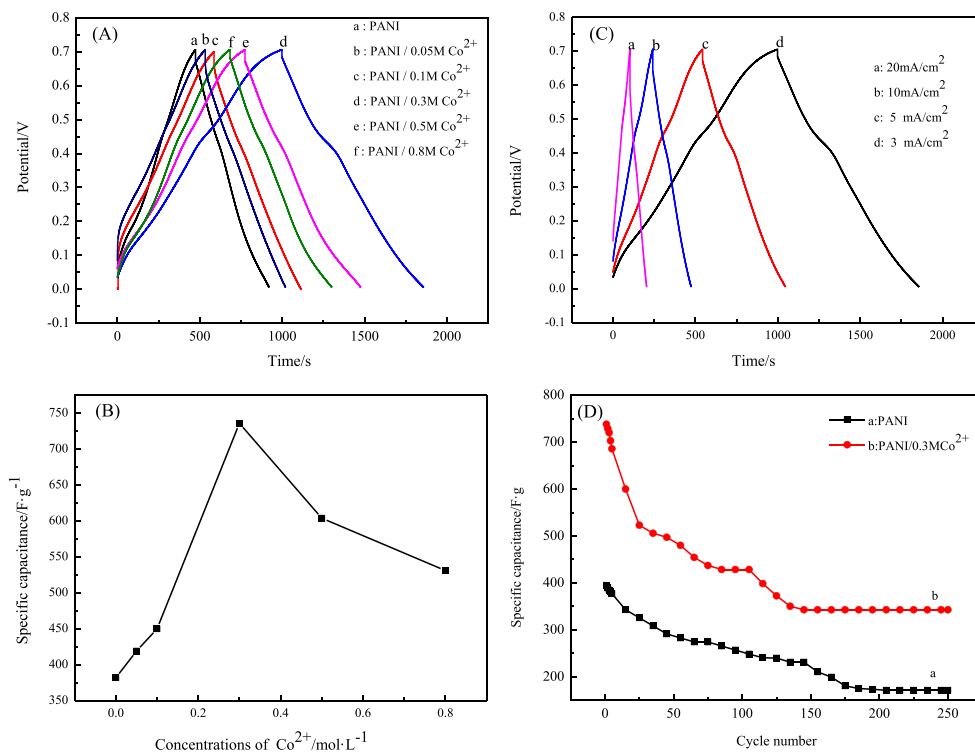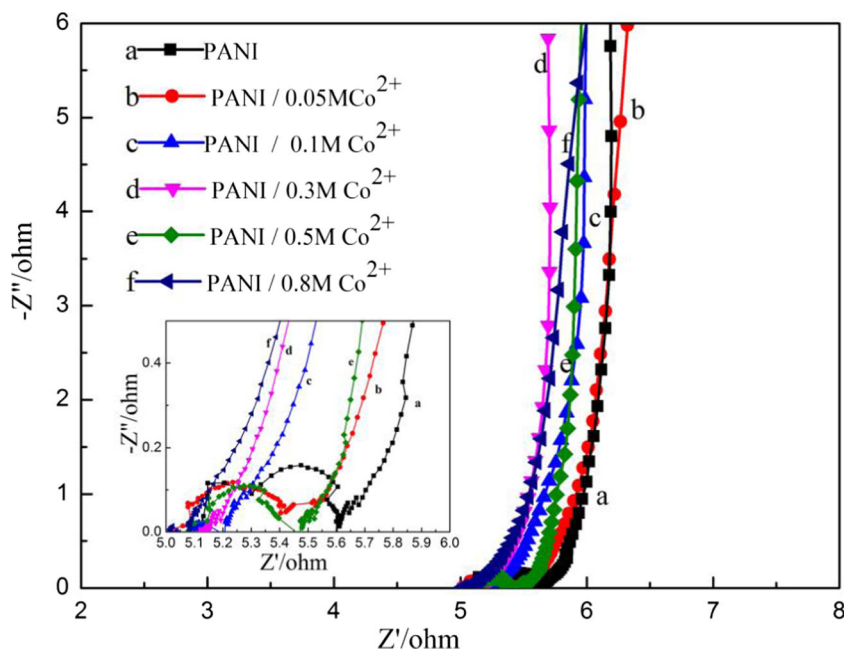
interaction between M^{n+} and PANI. However, with the doping transition metal ions continuous embedding and emergence, the volume of PANI expansion and contraction repeatedly which can cause the damage to the polymer chain, the doped PANI did not have a satisfactory cycleability. For practical application, the cycle stability of PANI remains to be further improved.

Electrochemical impedance spectroscopy Fig. 8 shows the electrochemical impedance spectra in the form of Nyquist plots for PANI and PANI/Co^{2+} films with the target of investigating the electrochemical behavior at the electrode/electrolyte interface. The impedance plots show a semicircle in the high-frequency region, where the high-frequency intercept of the semicircle on the real axis corresponds to the resistance of the electrolyte, the intrinsic resistance of the active material, and the contact resistance at the interface active material/current collector. The diameter of the semicircle provides a value of the charge–transfer resistance (R_{ct}) at the electrode/electrolyte interface, which depends on ion diffusion in the electrolyte to the electrode interface, and a tilted straight line in the low-frequency region represents a limiting

diffusion process in H_2SO_4 electrolyte, which shows the characteristic feature of ideal capacitive behavior [38]. As can be seen from Fig. 8, the charge transfer resistances estimated from the diameter of the semicircles are attributed to 0.51, 0.23, 0.18, 0.44, and 0.12 ohms with the increase of Co^{2+} ions. In general, the semicircle diameter of PANI/Co^{2+} is smaller than that of PANI, indicating that Co^{2+} has reduced the charge–transfer resistance. The almost vertical line suggests the ideally capacitive behavior of the electrodes.

To further confirm the influence of the nanostructure on the electrochemical performance, the equivalent circuit consisted with the above behaviors is showed in Fig. 9. The charge–transfer resistance of PANI and PANI/Co^{2+} films called R_{ct}, which has been described as a pseudo-charge–transfer resistance and a straight sloping line in the low-frequency range corresponding to the diffusive resistance. R_{sol} is the solution resistance in the circuit. Besides, the two constant-phase elements CPE_1 and CPE_2 are denoted as the double-layer capacitance and ionic diffusion process resulting in Warburg behavior in the electrode, respectively.
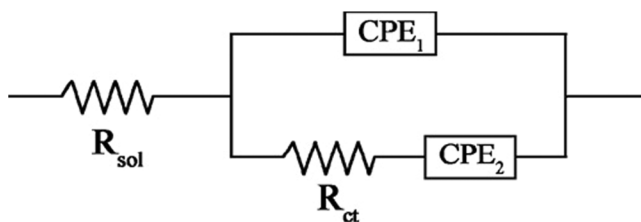

Fig 9 Equivalent circuit for the simulation of EIS spectra of PANI and PANI/Co^{2+} films

Conclusions

The PANI and PANI/Co^{2+} films were synthesized by cyclic voltammetry on a stainless steel wire mesh. The morphology and capacitive behavior of the composites were thoroughly studied. Compared with the pure PANI film, PANI/0.3 M Co^{2+} shows a larger specific capacitance of 736 F g^{-1} at a current density of 3 mA cm^{-2} and relatively good cycleability.

Accordingly, Co^{2+} has the positive role on the PANI, which can be considered as a potential way to improve the performance in supercapacitors.

References

1. Zheng Z, Huang L, Zhou Y, Hu XW, Ni XM (2009) Large-scale synthesis of mesoporous CoO-doped NiO hexagonal nanoplatelets with improved electrochemical performance. Solid State Sci 11: 1439–1443
2. Zhu JH, Chen MJ, Wei HG, Yerra N, Haldolaarachchige N, Luo ZP, Young DP, Ho TC, Wei SY, Guo ZH (2014) Magnetocapacitance in magnetic microtubular carbon nanocomposites under external magnetic field. Nano Energy 6:180–192
3. You Z, Shen K, Wu ZC, Wang XF, Kong XH (2012) Electrodeposition of Zn-doped α-nickel hydroxide with flower-like nanostructure for supercapacitors. Appl Surf Sci 258:8117–8123
4. Zhu JH, Chen MJ, He QL, Shao L, Wei SY, Guo ZH (2013) An overview of the engineered graphene nanostructures and nanocomposites. RSC Adv 3:22790–22824
5. Chen X, Wang HW, Yi H, Wang XF (2014) Anthraquinone on porous carbon nanotubes with improved supercapacitor performance. J Phys Chem C 118:8262–8270
6. Ryu KS, Kim KM, Park NG, Park YJ, Chang SH (2002) Symmetric redox supercapacitor with conducting polyaniline electrodes. J Power Sources 103:305–309
7. Xing SX, Zhao C, Jing SY, Wang ZH (2006) Morphology and conductivity of polyaniline nanofibers prepared by 'seeding' polymerization. Polym 47:2305–2313
8. Toupin M, Brousse T, Bélanger D (2004) Charge storage mechanism of MnO_2 electrode used in aqueous electrochemical capacitor. Chem Mater 16:3184–3190
9. Wei JT, Xing GZ, Gao L, Suo H, He XP, Zhao C, Li SA, Xing SX (2013) Nickel foam based polypyrrole–Ag composite film: a new route toward stable electrodes for supercapacitors. New J Chem 37:337–341
10. Shirakawa H, Louis EJ, MacDiarmid AG, Chiang CK, Heeger AJ (1977) Synthesis of electrically conducting organic polymers: halogen derivatives of polyacetylene, $(CH)_x$. J Chem Soc, Chem Commun 16:578–580
11. Burroughes JH, Bradley DDC, Brown AR, Marks RN, Mackay K, Friend RH, Burns PL, Holmes AB (1990) Light-emitting diodes based on conjugated polymers. Nat 347:539–541
12. Bélanger D, Ren X, Davey J, Uribe F, Gottesfeld S (2000) Characterization and long-term performance of polyaniline-based electrochemical capacitors. J Electrochem Soc 147:2923–2929
13. Gu HB, Wei HG, Guo J, Haldolaarachige N, Young DP, Wei SY, Guo ZH (2013) Hexavalent chromium synthesized polyaniline nanostructures: magnetoresistance and electrochemical energy storage behaviors. Polym 54:5974–5985
14. Gu HB, Guo J, Yan XR, Wei HG, Zhang X, Liu GR, Huang YD, Wei SY, Guo ZH (2014) Electrical transport and magnetoresistance in advanced polyaniline nanostructures and nanocomposites. Polym 55: 4405–4419
15. Javadi HH, Cromack KR, MacDiarmid AG, Epstein AJ (1989) Microwave transport in the emeraldine form of polyaniline. Phys Rev B 39:3579–3584
16. Wang YG, Joo J, Hsu CH, Epstein AJ (1995) Charge transport of camphor sulfonic acid-doped polyaniline and poly(o-toluidine) fibers: role of processing. Synth Met 68:207–211

17. SaravananS MCJ, Anantharaman MR, Venkatachalam S, Avasthi DK, Singh F (2005) Photoluminescence studies on RF plasma-polymerized thin films. Synth Met 155:311–315
18. Qiu B, Xu CX, Sun DZ, Wei HG, Zhang X, Guo J, Wang Q, Rutman D, Guo ZH, Wei SY (2014) Polyaniline coating on carbon fiber fabrics for hexavalent chromium removal. RSC Adv 4:29855–29865
19. Lu XH, Ng HY, Xu JW, He CB (2002) Electrical conductivity of polyaniline-dodecylbenzene sulphonic acid complex: thermal degradation and its mechanism. Synth Met 128:167–178
20. Wang CL, Sun L, Zhou Y, Wan P, Zhang X, Qiu JH (2013) P/N co-doped microporous carbons from H_3PO_4-doped polyaniline by in situ activation for supercapacitors. Carbon 59:537–546
21. Wei HG, Gu HB, Guo J, Wei SY, Liu GR, Guo ZH (2013) Silica doped nanopolyaniline with endured electrochemical energy storage and the magnetic field effects. J Phys Chem C 117:13000–13010
22. Qiu B, Xu CX, Sun DZ, Yi H, Guo J, Zhang X, Qu HL, Guerrero M, Wang XF, Noel N, Luo ZP, Guo ZH, Wei SY (2014) Polyaniline coated ethyl cellulose with improved hexavalent chromium removal. ACS Sustain Chem Eng 2(8):2070–2080
23. Li J, Cui M, Lai YQ, Zhang ZA, Lu H, Fang Jand Liu YX (2010) Investigation of polyaniline co-doped with Zn^{2+} and H^+ as the electrode material for electrochemical supercapacitors. Synth Met 160:1228–1233
24. Dhibar S, Sahoo S, Das CK, Singh R (2013) Investigations on copper chloride doped polyaniline composites as efficient electrode materials for supercapacitor applications. J Mater Sci Mater Electron 24:576–585
25. Xu H, Zhang JL, Chen Y, Lu HL, Zhuang JX (2014) Electrochemical polymerization of polyanilinne doped with Cu^{2+} as the electrode material for electrochemical supercapacitors. RSC Adv 4:5547–5552
26. Xu H, Li JL, Peng ZJ, Zhuang JX, Zhang JL (2013) Investigation of polyaniline films doped with Ni^{2+} as the electrode material for electrochemical supercapacitors. Electrochim Acta 90:393–399
27. Xu H, Zhang JL, Lu HL, Zhuang JX (2014) Electrochemical polymerization of polyanilinne doped with Zn^{2+} as the electrode material for electrochemical supercapacitors. J Solid State Electrochem 18:813–819
28. Sun T, Bi H, Zhu KR (2007) An infrared and raman spectroscopic study of polyanilines co-doped with metal ions and H^+. Spectrochim Acta Part A 66:1364–1368
29. Kim YH, Foster C, Chiang J, Heeger AJ (1989) Localized charged excitations in polyaniline: infrared photoexcitation and protonation studies. Synth Met 29:285–290
30. Moon YB, Cao Y, Smith P, Heeger AJ (1989) X-ray scattering from crystalline polyaniline. Polym Commun 30:196–199
31. Yang CM, Chen CY (2005) Synthesis, characterisation and properties of polyanilines containing transition metal ions. Synth Met 153:133–136
32. Kim JG, Pugmire DL, Battaglia D, Langell MA (2000) Analysis of the $NiCo_2O_4$ spinel surface with Auger and X-ray photoelectron spectroscopy. Appl Surf Sci 165:70–84
33. Trung T, Trung TH, Ha CS (2005) Preparation and cyclic voltammetry studies on nickel-nanoclusters containing polyaniline composites having layer-by-layer structures. Electrochem Acta 51:984–990
34. Wang YG, Li HQ, Xia YY (2006) Ordered whiskerlike polyaniline grown on the surface of mesoporous carbon and its electrochemical capacitance performance. Adv Mater 18:2619–2623
35. Li GR, Feng ZP, Zhong JH, Wang ZL, Tong YX (2010) Electrochemical synthesis of polyaniline nanobelts with predominant electrochemical performances. Macromol 43:2178–2183
36. Alemany P, Casanova D, Álvarez S (2012) Continuous symmetry measures of irreducible representations: application to molecular orbitals. Phys Chem Chem Phys 14:11823–11886
37. Wang YG, Xia YY (2006) Hybrid aqueous energy storage cells using activated carbon and lithium-intercalated compounds: the $C/LiMn_2O_4$ System. J Electrochem Soc 153:A450–A454
38. Wei HG, Zhu JH, Wu SJ, Wei SY, Guo ZH (2013) Electrochromic polyaniline/graphite oxide nanocomposites with endured electrochemical energy storage. Polym 54:1820–1831